

M²I Communication: From Theoretical Modeling to Practical Design

Hongzhi Guo and Zhi Sun

State University of New York at Buffalo, Buffalo, NY, USA
{hongzhig, zhisun}@buffalo.edu

Abstract—Wireless communications in complex environments are constrained by lossy media and complicated structures. Magnetic Induction (MI) has been proved to be an efficient solution to extend the communication range. Due to the small coil antenna's physical limitation, however, MI's communication range is still very limited. To this end, Metamaterial-enhanced Magnetic Induction (M²I) communication has been proposed and the theoretical results suggest that it can significantly increase the communication performance, namely, data rate and communication range. Nevertheless, currently, the real implementation of M²I is still a challenge and there is no guideline on design and fabrication of spherical metamaterial. In this paper, we propose a practical design by using a spherical coil array to realize M²I and we prove that it can achieve negative permeability and there exists a resonance condition where the radiated magnetic field can be significantly amplified. The radiation and communication performance are evaluated and full-wave simulation in COMSOL Multiphysics is conducted to validate the design objectives. By using the spherical coil array-based M²I, the communication range can be significantly extended, exactly as we predicted in the theoretical model.

I. INTRODUCTION

Although terrestrial wireless communication has been well developed and extensively utilized, its counterpart in complex environments, such as underground, oil reservoirs and nuclear plants, is still in its infancy. Wireless communication in such environments can enable a large number of important applications, such as harsh environment monitoring by using wireless sensors, miners rescue, and mitigation in nuclear plants using robots. Wireless signals in complex environments suffer from high absorption and multiple scattering which results in significant propagation loss. Therefore, extremely large antenna and high transmission power have to be used to accomplish signal transmissions. However, the devices for wireless communication is becoming smaller and smaller, such as sensors for wireless sensor networks and portable devices for wireless area networks. These devices can not be equipped with such large antennas or provide enough power. As a result, a new communication mechanism is highly desired to solve this problem.

Magnetic Induction (MI) as a promising solution has been envisioned to enable long-distance wireless communications in underground [1] and underwater [2]. Wireless signals are transmitted by using the reactive power constrained in the near field of a coil rather than using the propagating wave. Thus, it suffers from lower propagation loss and signal delay. Also, it enjoys a stable channel since the permeability is the same for most of the natural materials. Even the generated power by a coil antenna attenuate slower than that by an electrical antenna, the intrinsic physical limitation of the highly inductive coil antenna prevents further improving its efficiency [3]. Metamaterial is

introduced to MI in [4], where an ideal negative-permeability metamaterial shell is utilized to surround a loop antenna, as shown in Fig. 1. The near-field reactive power generated by the loop antenna can be matched by a metamaterial shell. The theoretical results predict that a pocket-size loop antenna can achieve around 20 m communication range with high data rate. However, since the considered metematerial in [4] is ideally homogeneous and isotropic which is not available in reality, a practical design is highly desired to validate the theoretically predicted results.

Metamaterial is composed of periodic artificial metallic or dielectric atoms. It can demonstrate negative permeability and permittivity, which can manipulate electromagnetic waves in extraordinary ways [5]. The periodic metamaterial components can be organized in many ways. In [6], metamaterial unit cells formed a slab which is utilized for high-efficiency wireless power transmission. The ideal model in the seminal work [7] is realized by using compact structure in [8]. In [9], a metamaterial cylindrical shell is fabricated to improve the accuracy of Magnetic Resonance Imaging (MRI). More relevantly, most of existing works on metamaterial cloaking at GHz or THz bands, which makes the objects inside a spherical shell invisible, consider the ideally homogeneous metamaterial. Currently, it is still a great challenge to make metamaterial spherical. Besides the shape, since metamaterial is a kind of effective media [10], the effective parameters, such as effective permeability and thickness, are hard to extract. Since in [4], the high efficiency of M²I strongly depends on the negative permeability and thickness, it is crucial to find them out.

In this paper, the ideally theoretical model of Metamaterial-enhanced Magnetic Induction (M²I) communication in [4] is pushed forward to a practical design. Specifically, we substitute the ideally homogeneous and isotropic metamaterial with a spherical coil array to realize M²I. A large number of small coils are uniformly placed on a spherical shell to enhance the radiated field by a loop antenna, which in turn increases the communication range and data rate. We prove that this spherical coil array can achieve negative permeability. In addition, the optimal configuration of the proposed spherical coil array is found and its communication performances are similar as the ideal M²I in [4], both of which are much better than the original MI [1]. The results are evaluated and validated by full-wave simulations.

The following of this paper is organized as follows. First, the theoretical details of the ideal M²I is reviewed in Section II. After that, a practical design of M²I is discussed in Section III. Next, the wireless communication performance by using practical M²I are presented in Section IV. Finally, this paper is concluded in Section V.

This work was supported by the US National Science Foundation (NSF) under Grant No. 1547908.

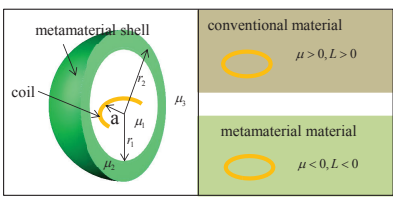


Fig. 1. Illustration of M^2I .

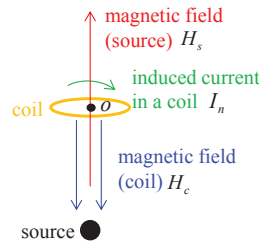


Fig. 2. Illustration of effective μ .

II. THEORETICAL MODELING OF M^2I

M^2I was proposed in our previous work [4] to extend the magnetic induction communication range in complex environments, such as underwater and underground. The geometric structure is illustrated in Fig. 1. A loop antenna is enclosed by a metamaterial shell with thickness $r_2 - r_1$. The permeability of the inner layer, metamaterial layer and outer layer are denoted by μ_1 , μ_2 and μ_3 , respectively. Also, the metamaterial layer is considered as ideally homogeneous and isotropic. The key parameter of MI communication is the mutual inductance, which couples the transmitting and receiving antenna together. By using M^2I , the mutual inductance can be expressed as [4]

$$M_0 = \frac{\mathcal{F}_1}{\mathcal{S}_m^2}, \text{ where}$$

$$\bar{S}_m = \mathcal{F}_2 \underbrace{\left[2r_1^3(\mu_1 - \mu_2)(\mu_3 - \mu_2) - r_2^3(2\mu_2 + \mu_1)(2\mu_3 + \mu_2) \right]}_{\mathcal{F}_3} + \hat{o}, \quad (1)$$

\mathcal{F}_1 and \mathcal{F}_2 are coefficients, and \hat{o} is an asymptotically small value. The first item on the right-hand side of (1) is much larger than \hat{o} . When \mathcal{F}_3 is zero, \bar{S}_m can be minimized, which in turn maximizes M_0 . Therefore, if the outer shell radius r_2 , inner permeability μ_1 and outer permeability μ_3 are determined, by adjusting metamaterial shell's thickness r_1 and permeability μ_2 , we can always satisfy the condition to maximize M_0 . This enhancement is because of the matching between the metamaterial layer and the coil antenna[7], [8]. As depicted on the right-hand side in Fig. 1, a coil in conventional materials has a positive self-inductance L , while L becomes negative when the coil is in metamaterials due to the negative permeability. Intuitively, we can use metamaterials to match with conventional materials to reduce the reactive power in vicinity of a loop antenna.

III. PRACTICAL DESIGN OF M^2I SHELL

In this section, an approach is presented to achieve the negative permeability, upon which we propose a spherical structure to obtain the negative permeability.

A. Negative Permeability

When a mixture's components are much smaller than wavelength, the mixture can be regarded as an effectively homogeneous medium and its constitutive parameters, such as effective permeability, permittivity and conductivity, can be found [10]. First, by using a coil as an example, we show the way to obtain the effective permeability.

As shown in Fig. 2, a source radiates magnetic field $H_s \hat{s}$ which can induce current I_s in a coil whose center is a point o . Here, \hat{s} is a unit vector standing for the direction of magnetic field. If we consider there is no coil, at point o ,

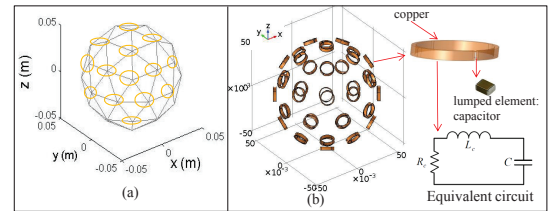


Fig. 3. Spherical coil array. (a) Pentakis icosidodecahedron with 42 vertices; each vertex is the center of a coil; the orientation of a coil is the radial direction from the center of the sphere to the corresponding vertex. (b) 3D model and equivalent circuit.

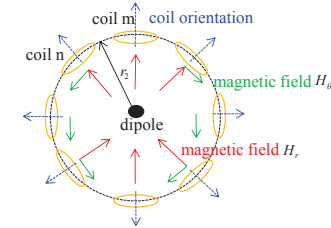


Fig. 4. Illustration of coil orientation and the direction of magnetic field radiated by a magnetic loop antenna.

the magnetic flux can be expressed as $B_m = \mu_0 H_s \hat{s}$, where μ_0 is the permeability of vacuum. However, if the coil exists, due to the induced current I_s , the coil reradiates magnetic field $H_c \hat{c}$, where \hat{c} is also a unit vector denoting the direction of the reradiated magnetic field. As a result, the magnetic flux at point o can be updated as

$$B_m = \mu_0 H_s \hat{s} + \mu_0 H_c \hat{c} = \mu_0 \left(1 + \frac{H_c \hat{c}}{H_s \hat{s}} \right) H_s \hat{s} = \mu_{eff} H_s \hat{s}, \quad (2)$$

where μ_{eff} is the effective permeability at point o .

From (2) we can see, the effective permeability can be controlled provided that we can manipulate the reradiated magnetic field $H_c \hat{c}$. When $\frac{H_c \hat{c}}{H_s \hat{s}}$ is negative and its absolute value is larger than 1, the negative permeability can be obtained.

B. Spherical M^2I Shell

The geometrical structure of the spherical coil array is presented in Fig. 3. The same as our discussion in [4], we set the outer radius of the spherical shell as 0.05 m. By using the Pentakis icosidodecahedron [11], we equally divide the surface of the sphere into 80 triangles with 42 vertices. Each vertex is the center of a coil and the coil's orientation is the radial direction from the center of the shell to the vertex. In this way, the coil array is constructed by 42 identical coils. The realistic 3D model is demonstrated in Fig. 3(b). The coils are made of copper wires with capacitors to tune them. In the equivalent circuit L_c , R_c , and C represent the coil inductance, coil resistance, and capacitance, respectively.

1) Effective Permeability of M^2I Shell: First, the spherical coil array are considered as a homogeneous layer. By using Effective Medium Theory [5], we find the effective permeability of this layer. All the coils on the shell are passive and they are excited by a loop antenna at the center of the shell, as shown in Fig. 4. According to Kirchhoff voltage law we can

obtain,

$$\underbrace{\begin{bmatrix} Z_1 & j\omega M_{12} & \cdots & j\omega M_{1N} \\ j\omega M_{21} & Z_2 & \cdots & j\omega M_{2N} \\ \vdots & \vdots & \ddots & \vdots \\ j\omega M_{N1} & j\omega M_{N2} & \cdots & Z_N \end{bmatrix}}_{\mathbf{Z}} \cdot \underbrace{\begin{bmatrix} I_1 \\ I_2 \\ \vdots \\ I_N \end{bmatrix}}_{\mathbf{I}} = \underbrace{\begin{bmatrix} V_1 \\ V_2 \\ \vdots \\ V_N \end{bmatrix}}_{\mathbf{V}} \quad (3)$$

where N is the number of coils on the shell, $Z_n = R_c + j\omega L_c + 1/j\omega C$, M_{mn} is the mutual inductance between coil m and coil n and the detailed calculation is provided in Appendix A, I_n is the induced current in coil n , and V_n is the voltage. The magnetic field radiated by a loop antenna can be expressed as [12]

$$H_r(I_0) = \hat{H}_r \cos \theta \hat{r}_0 = \frac{jka^2 I_0 \cos \theta}{2d^2} \left[1 + \frac{1}{jkd} \right] e^{-jkd} \hat{r}_0, \quad (4)$$

$$H_t(I_0) = \frac{-k^2 a^2 I_0 \sin \theta}{4d} \left[1 + \frac{1}{jkd} - \frac{1}{(kd)^2} \right] e^{-jkd} \hat{\theta}_0, \quad (5)$$

where a is the radius of a coil, k is the wavenumber, d is the distance from the coil's center, θ is the azimuthal angle, and \hat{r}_0 and $\hat{\theta}_0$ are unit vectors representing the radial and azimuthal direction, respectively. The direction of H_r and H_t are depicted in Fig. 4. Since the coil orientation is parallel with H_r 's direction and perpendicular to H_t 's direction, only H_r can induce currents in the coils on the shell. As a result, this shell can be regarded as metamaterial for H_r , but not for H_t . In our future work, a tri-directional coil [13] will be adopted to make the coils on the shell isotropic but it's out of the scope of this paper. Accordingly, V_n can be expressed as

$$V_n = -j\omega \pi a^2 \mu_0 \hat{H}_r \cos \theta_n, \quad (6)$$

where \hat{H}_r can be derived from (4) and it is the same for all the coils on the shell. According to Kirchhoff's voltage law, without loss of generality, in coil n we can obtain

$$I_n(R_c + j\omega L_c - j/\omega C) + \sum_{i=1, i \neq n}^N j\omega M_{in} I_i = -j\omega \pi a^2 \mu_0 \hat{H}_r \cos \theta_n. \quad (7)$$

By rearranging (7) we have,

$$\frac{I_n(R_c + j\omega L_c + 1/j\omega C)}{\hat{H}_r \cos \theta_n} = -j\omega \pi a^2 \left(\sum_{i=1, i \neq n}^N \frac{M_{in} I_i}{\pi a^2 \hat{H}_r \cos \theta_n} + \mu_0 \right). \quad (8)$$

In addition, we have the following proposition:

Proposition 1: For any coil n on the shell, $I_n = \mathcal{A} \hat{H}_r \cos \theta_n$, where \mathcal{A} is a constant.

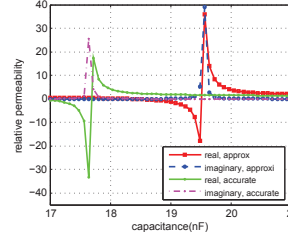
Proof: See Appendix B. \blacksquare

If only coil n exists on the spherical shell and all other coils are removed, there is only μ_0 in the bracket on the right-hand side of (8). In other words, the first item in the bracket denotes the mutual interactions among coils on the shell. When there are no other coils, this item does not exist and this is indeed the conventional material with permeability μ_0 . Hence, when we consider all other coils on the shell, the terms in the bracket can be regarded as the effective permeability. In addition, based on Proposition 1, since $\frac{I_n}{\hat{H}_r \cos \theta_n} = \mathcal{A}$, the left-hand side of (8) is a constant. Therefore, no matter which coil on the shell we choose, the value in the bracket does not change, i.e., the effective permeability is homogeneous. By using (8) and the value of \mathcal{A} in Appendix B, we can obtain

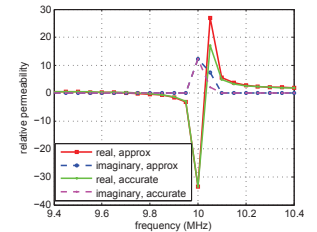
$$\mu_{eff} = \left(1 - \frac{j\omega \sum_{i=1, i \neq n}^N M_{in}}{R_c + j\omega L_c + 1/j\omega C + \sum_{i=1, i \neq n}^N j\omega M_{in}} \right) \mu_0. \quad (9)$$

TABLE I. SIMULATION PARAMETERS

μ_0	$4\pi \times 10^{-7}$ H/m	ϵ_0	8.854×10^{-12} F/m	L_{app}	13.8 nH
f	10 MHz	a	0.007 m	L_c	15.2 nH
r_2	0.05 m	R_c	0.244 m Ω		



(a) Effect of capacitance



(b) Effect of frequency

Fig. 5. Effective permeability.

From (9) we can see when the second item in the bracket is larger than 1, a negative permeability can be achieved. Moreover, from (9) we can find that the effective permeability is only determined by the coils' mutual inductances and the lumped elements. It is not affected by the source. Based on (9), we numerically evaluate the effective permeability of the spherical coil array. The numerical parameters of the system are provided in Table I. Note that in Table I, $L_{app} = \frac{\pi \mu_0 a}{2}$ is the approximated self-inductance and L_c is the accurate value measured in COMSOL. L_{app} is utilized to obtain a succinct closed-form formula to elucidate physics better.

The effective permeability is shown in Fig. 5. Due to the resistance of coils, the effective permeability is a complex number where the imaginary part stands for the loss in coils. First, we set the frequency as 10 MHz to investigate the effect of capacitance. As depicted in Fig. 5(a), the approximated and accurate self-inductance has the same trend but there is a little shift. Moreover, when the capacitance is small, the impedance of the capacitor is large since $Z_c = \frac{1}{j\omega C}$. Therefore, the relative permeability is negative as discussed in Section II. When the capacitance is large, the inductance is dominant. Then, the relative permeability becomes positive. Also, there is a dramatic change from negative to positive. The reason is that around the resonant point, the capacitor and inductor are almost perfectly matched. Hence, the reactance is very small and the current in each coil is significant. A slight change of the capacitance or inductance can greatly change the current direction in the coil.

Then, we set the capacitance as 17.6 nF for the accurate self-inductance and 19.5 nF for the approximated self-inductance to investigate the effect of frequency. As shown in Fig. 5(b), by using the approximated and accurate self-inductance, they have almost the same performance since both of them are tuned at 10 MHz. Furthermore, a large negative effective permeability is obtained at 10 MHz. However, the imaginary part of the permeability is also very large which reduces the merit of this point. Also, we notice that changing capacitance is similar as changing frequency since in (9), ω and C have the same effect on the impedance of the capacitor.

IV. CHARACTERIZING M²I COMMUNICATION UNDER PRACTICAL DESIGN

In this section, the communication performance of spherical coil array-based M²I is evaluated and compared with the original MI. The key factor of MI communication, i.e., magnetic field intensity, is discussed first. Then, the path loss, bandwidth and channel capacity of M²I channel are presented.

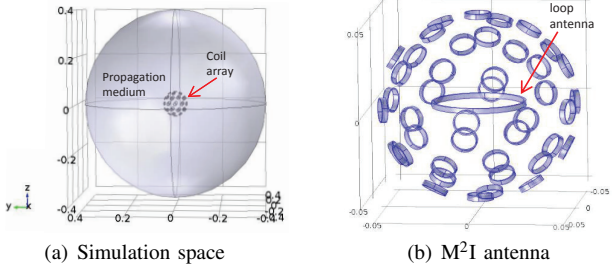


Fig. 6. Geometry of full-wave simulation in COMSOL Multiphysics.

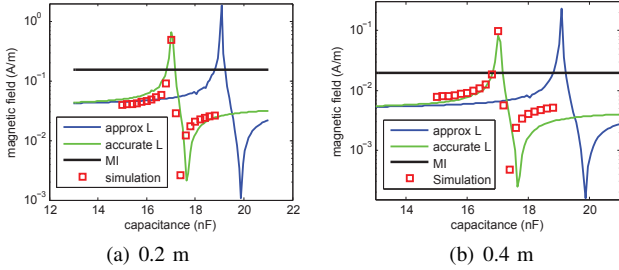


Fig. 7. Magnetic field (A/m) at a distance 0.2 m and 0.4 m from the center of the shell.

Note that, the radius of the loop antenna inside a spherical coil array is set as 0.025 m, while the radius of MI loop antenna is set as 0.05 m, i.e., the outer radius of the coil array shell. In other words, they occupy the same space. Also, the ideal M^2I 's performance is not comparable with coil array-based M^2I even they have the same negative permeability. Because the inner radius of ideal M^2I in [4] is 0.025 m and the loop antenna is 0.015 m in radius. However, the coil array-based M^2I has almost no physical thickness. As a result, we can set the loop antenna much larger than ideal M^2I to fully use the space. Even the physical thickness of practical M^2I is small, in this section, we would show that the effective thickness and permeability are equivalent to the lumped capacitor, which can be adjusted to find the optimal configuration.

A. Magnetic Field Analysis

1) Radiated Magnetic Field: In this part, we put a loop antenna into the shell to evaluate its performance. The geometric model of both theory and simulation is demonstrated in Fig. 6. Only the large loop antenna is actively excited and all other small coils on the shell are passive.

Since the induced power in the receiving coil is proportional to magnetic field intensity, we use this intensity as a metric to show the enhancement. Note that (4) can be applied when the coordinates origin is the center of the coil and z-axis overlaps the coil's orientation vector. At the observation point O , we first consider all the fields from each antenna individually. Then we decompose the fields in a Cartesian coordinates. Finally, we add all the fields together. As a result, the magnetic field at point O can be found. The radiated magnetic field is the summation of the radiated magnetic field by the loop antenna and reradiated magnetic fields by the passive coils on the shell, which can be expressed as

$$H = \sum_{i=0}^N [H_r(I_i)\hat{r}_i + H_t(I_i)\hat{\theta}_i], \quad (10)$$

where the large loop antenna is denoted by $i = 0$, and the induced current can be determined by using (3).

2) Magnetic Field Enhancement: The radiated field is evaluated in this part. The radius of the loop antenna is set as 0.025 m and its current is set as 1 A. The MI antenna with

a larger radius 0.05 m, i.e., the outer radius of the shell, is excited with the same current. Then, we compare the radiated magnetic field intensity at 0.2 m and 0.4 m from the center of M^2I and MI loop antennas. Since the dipole moment is $\pi a^2 I_0$, the MI loop antenna's dipole moment is 4 times larger than M^2I loop antenna. The effect of C on the field intensity is investigated. Also, the magnetic field is measured along z-axis since H_r is dominant.

As shown in Fig. 7, by using the accurate self-inductance, the theoretical result agrees well with the full-wave simulation. Also, by using the approximated self-inductance, it does not affect the trend of the resonance. The coil array-based M^2I can provide almost one order gain. Referring to Fig. 5(a), it is interesting to find that the highest magnetic field intensity does not appear at the most negative or positive effective permeability. The strongest field intensity is obtained when the effective permeability is a little smaller than 0. The reason can be interpreted from two aspects. On the one hand, we need a negative permeability to match with the inductive source. According to (11), by adjusting C , we can always find the resonance. On the other hand, when the effective permeability becomes more negative, the imaginary part of the permeability increases dramatically which deteriorates the performance. Therefore, we have to strike a balance between the negative permeability and low loss, i.e., small imaginary part of the effective permeability. Additionally, by comparing Fig. 7(a) and Fig. 7(b), we find that the gain from this coil array-based M^2I does not change with distance which can validate that this gain is from radiation, but not near field induction. In Fig. 8, we compare the radiated field by M^2I coil array (outer radius is 0.05 m) and original large MI antenna (radius is 0.05 m). Due to the high computation burden in COMSOL, we show the simulated magnetic field intensity within 1 m. The results further prove that the gain is a constant with distance change.

3) Resonance Condition: In order to enhance the magnetic field, we need to maximize I_n to enlarge the reradiated field by the coils. In (9), the second item in the bracket can be maximized when the reactive terms on the denominator are eliminated. Therefore, by letting $j\omega L_c + 1/j\omega C + \sum_{i=1,i\neq n}^N j\omega M_{in} = 0$ and $L_c \approx L_{app} = \frac{\mu_{ra}}{2}$, we can obtain

$$\frac{a}{r_2} \approx \sqrt[3]{\frac{1}{15.3} \left(\frac{1}{2} - \frac{1}{\omega^2 \mu_0 \pi a C} \right)}. \quad (11)$$

In [4], by adjusting the thickness and negative permeability, we can achieve a resonance to amplify the magnetic field intensity. In this paper, when all other configurations are fixed, by adjusting the capacitor C we can also achieve this resonance, as suggested by (11). Since the negative permeability metamaterial is equivalent to capacitor as discussed in Section II, they have the same physical principles. Therefore, changing C is equivalent to changing both the thickness and the negative permeability.

4) Negative Self-Inductance: It is also interesting to notice that there is a dramatic decrease of field intensity after the resonance point in Fig. 7, i.e., around 17.5 nF for the accurate L and 20 nF for the approximated L . In [4], we found a negative self-inductance and the reason is explained theoretically. The results are also validated in Fig. 14 and Fig. 16 in [4]. Since the self-inductance changes from positive to negative then it changes back from negative to positive, there exists two points where the self-inductance is almost 0. Here, by using a practical M^2I , we find the same negative self-inductance and the dramatic decrease of magnetic field intensity is because of

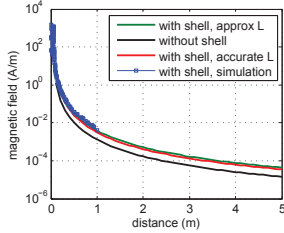


Fig. 8. Distance effect on Magnetic field intensity.

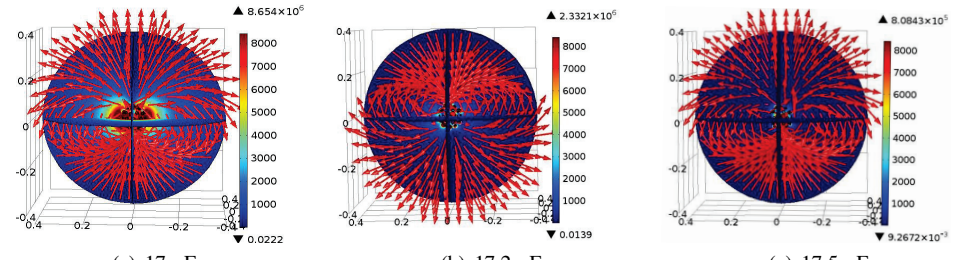


Fig. 9. Simulation results of magnetic field direction close to resonance condition.

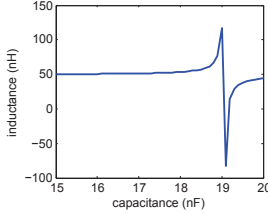


Fig. 10. Self-inductance

it. In the following, we explain the reason of this negative self-inductance from the perspective of practical design instead of ideal metamaterial.

By using the full-wave simulation results in COMSOL, which are shown in Fig. 9, we explain how the negative self-inductance is generated. When $C=17$ nF, the magnetic field intensity is large and the self-inductance is positive since the reradiated magnetic field and the magnetic field radiated by the loop antenna have the same direction. However, if we increase C to 17.2 nF, the magnetic field changes its direction and the self-inductance becomes negative. Referring to Fig. 2, when H_c is larger than H_s , the overall magnetic field changes its direction from H_s to H_c . In other words, when $1/j\omega C$ is smaller than $j\omega L$ and the the reradiated magnetic field from the shell is larger than the original magnetic field radiated by the loop antenna, the total field radiated from the coil array will change its direction. Note that, here Right-hand rule no longer validates, since a positive current in the loop antenna generates a magnetic field obeys Left-hand rule. Therefore, the self-inductance is negative. When we further increase C to 17.5 nF, the self-inductance changes to positive again since the resonance does not exist and the currents in the coils are much smaller than the current in the loop antenna. Thus, when the self-inductance gradually changes from negative to positive, there is a region where its value is around zero which makes the radiated field extremely small. However, the change from positive to negative is dramatic and this effect is not obvious. The effective self-inductance $L_{eff} = L_{app} + \Im(Z_{ref})/j\omega$, where \Im denotes the imaginary part of a complex number, is also plotted in Fig. 10. It shows the negative self-inductance is at around 19 nF. Due to the coupling among the loop antenna in the shell and coils on the shell, the reflected impedance in the loop antenna need to be considered which can be expressed as [1] $Z_{ref} = \sum_{i=1}^N \frac{\omega M_{0i}^2}{Z_i}$, where the subscript 0 denotes the loop antenna. The negative self-inductance generated by the spherical coil array is consistent with the discussion in [4], i.e., Fig. 14 and Fig. 16, by using the ideal metamaterial.

B. Wireless Channel Analysis

Up to this point, we have demonstrated that the coil array-based M²I can significantly enhance the radiated magnetic field

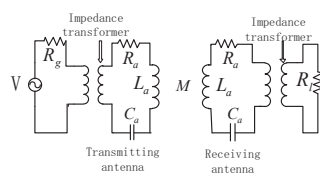


Fig. 11. Equivalent circuit

intensity. In this section, we present the performance of the wireless channel between two M²I transceivers, i.e., both the transmitter and receiver are equipped with coil array-based M²I antenna.. In particular, the path loss, bandwidth and channel capacity are discussed.

1) Path Loss: The equivalent circuit is shown in Fig. IV-A4, where R_g and R_l are the source's output resistance and load resistance, respectively. Both of the R_g and R_l are set as a typical value 50 Ω. The impedance transformer is utilized for impedance matching between the source/load and antenna. The resistance, self-inductance and tunable capacitance in the antenna circuit are denoted by R_a , L_a , and C_a , respectively. When we compare the M²I transceivers and original MI transceivers, the same as previous discussions, the radius of the original MI antenna is the outer radius of the shell, i.e., 0.05 m. In order to calculate the magnetic field at the receiving side, we need to add the passive coils in the receiving M²I antenna into (3) and (10). Now, we have a transmitting antenna, 84 passive coils, and a receiving antenna. Therefore, the updated dimensions of \mathbf{Z} , \mathbf{I} and \mathbf{V} in (3) are 86×86, 86×1, and 86×1, respectively.

Then the inductance in the loop antenna is matched by a tunable capacitor C_a . The resistance is matched by the impedance transformer: $N_1^2 \cdot [R_a + \Re(Z_{ref})] = R_g \cdot N_2^2$ where \Re stands for the real part of a complex number, and N_1 and N_2 are the primary and secondary turns, respectively. Therefore, the voltage for the transmitting loop antenna is $V_0 = VN_2/2N_1$. All other voltages in the updated (3) are 0. By solving the updated (3), the induced current in antennas can be found. The received power can be expressed as $P_r = |I_l|^2 R_l$, where I_l is the load current. Similarly, the dissipated power in the source can be expressed as $P_t = V^2/2R_g$. Then, we can obtain the path loss $\mathcal{L}(d) = -10\lg(P_r/P_t)$.

Next, by using the approximated self-inductance L_{app} and letting $C=19.06$ nF (optimal value find in Fig. 7), we compare the performance of coil array-based M²I with that of the original MI. Also, the loop antenna resistance are set as 0.1 Ω and 0.2 Ω for coil array-based M²I (antenna radius 0.025 m) and the original MI (antenna radius 0.05 m), respectively. As shown in Fig. 12(a), the path loss of M²I is much lower than that of original MI which is consistent with [4].

2) Bandwidth: In order to investigate the frequency response of the system, we keep the distance between a transmitter and a receiver as 3 m and 6 m and vary the frequency. As shown in Fig. 12(b), the enhancement of M²I greatly reduces the bandwidth since magnetic field intensity is strongly based on resonance. The 3 dB bandwidth for M²I is 4 kHz, while it is 320 kHz for original MI. Also, we notice that changing frequency is consistent with changing capacitance. When frequency is higher than the designed frequency, the signal strength drops fast. Moreover, at 3 m and 6 m, the

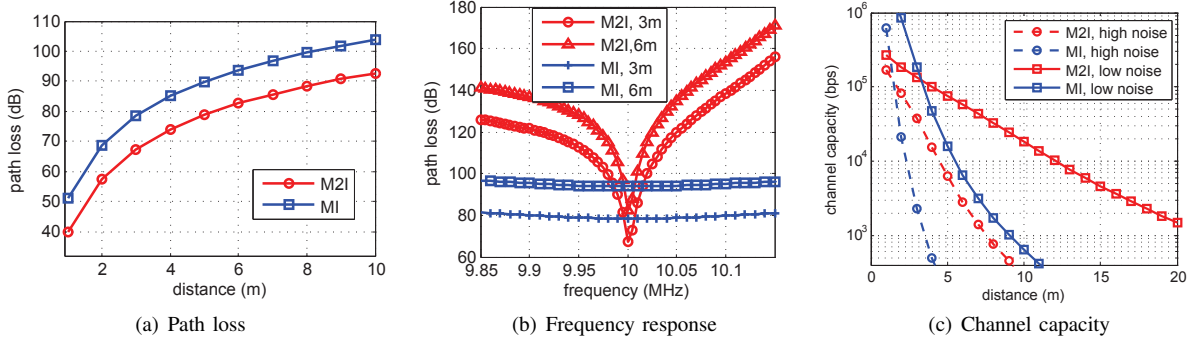


Fig. 12. Communication performance.

bandwidth are almost the same, which implies that it is not affected by distance.

3) Channel Capacity: The Shannon channel capacity is also evaluated. According to, $C = Bw \cdot \log_2[1 + P_r/(Bw \cdot N_{noise})]$, where Bw is the bandwidth and N_{noise} is the noise density. We set the transmission power as 10 dBm and consider two noise levels, namely, high noise -110 dBm/Hz and low noise -130 dBm/Hz. As it shown in Fig. 12(c), M²I can increase the communication range significantly. Besides the low path loss of M²I, the narrower bandwidth also brings lower noise power.

V. CONCLUSION

Metamaterial has been introduced to enlarge magnetic induction's communication range and data rate. However, the existing works are based on ideal metamaterial model. In this paper, we propose a practical design of Metamaterial-enhanced Magnetic Induction (M²I) communication by using a spherical coil array. The physical principles and geometric structure of this design are introduced. The relation between this practical M²I and the ideal metamaterial based M²I are discussed. Through the communication performance evaluation, we find it can significantly increase the channel capacity, which in turn extends the communication range greatly.

APPENDIX

A. Mutual Inductance

The mutual inductance utilized in eqs. (3) and (7) to (9) is derived here. Without loss generality, the mutual inductance between coil 0 and coil 1 can be denoted as M_{01} , where coil 0 is transmitting coil and coil 1 is receiving coil. We can find the magnetic field intensity radiated by coil 0 by using (4). Let the magnetic field intensity at coil 1 be $H_0\hat{h}$, where \hat{h} is the magnetic field direction. Then the mutual inductance can be expressed as $M_{01} = \mu_0 H_0 \pi a_1^2 \hat{h} \cdot \hat{\delta}_1 / I_0$, where a_1 is the radius of coil 1, I_0 is the current in coil 0, and $\hat{\delta}_1$ is the orientation unit vector of coil 1.

B. Proof of Proposition 1

First, in (7) $\mathbf{Z}\mathbf{I}_0 = \mathbf{V}_0$. Assume that all the elements in \mathbf{V}_0 are the same, i.e., $V_1 = V_2 = \dots = V_N = -j\omega\pi a_1^2 \mu_0 \hat{H}_r$. Since all the coils are uniformly distributed on the spherical shell, the structure is symmetrical. Moreover, as the coils have the same excitation voltages, they should have the same induced currents, i.e., $I_1 = I_2 = \dots = I_N$. Equation (7) reduces to $I_1(Z_1 + \sum_{i=1}^N j\omega M_{1i}) = V_1$. Thus, $I_1 = \mathcal{A}\hat{H}_r$, where $\mathcal{A} = \frac{-j\omega\pi a_1^2 \mu_0}{R_c + j\omega L_c + 1/j\omega C + \sum_{i=1, i \neq n}^N j\omega M_{in}}$ is a constant. Since the coils are uniformly distributed, $\sum_{i=1, i \neq n}^N j\omega M_{in}$ are the same for all

the coils no matter which n we choose. Then, we consider the source is a magnetic loop antenna and (7) is updated as $\mathbf{Z}\hat{\mathbf{I}} = \hat{\mathbf{V}}$. According to (6), $V_n = \mathcal{A}\hat{H}_r \cos \theta_n$. Hence $\hat{\mathbf{V}} = \mathbf{K}\mathbf{V}_0$, where \mathbf{K} is a diagonal matrix and $\text{diag}(\hat{\mathbf{K}}_n) = \cos \theta_n$. Thus, $\mathbf{Z}\hat{\mathbf{I}} = \mathbf{K}\mathbf{V}_0$. By multiplying the inverse of \mathbf{K} , we can obtain $\mathbf{K}^{-1}\mathbf{Z}\hat{\mathbf{I}} = \mathbf{V}_0$. Also, \mathbf{Z} can be regarded as diagonal matrix since mutual inductances are much smaller than coil impedances, i.e., $j\omega M \ll (R_c + j\omega L_c - j/\omega C)$. Thus, $\mathbf{Z}\mathbf{K}^{-1}\hat{\mathbf{I}} = \mathbf{V}_0$ and $\mathbf{I}_0 = \mathbf{K}^{-1}\hat{\mathbf{I}}$. Then, we can obtain $\hat{\mathbf{I}} = \mathbf{K}\mathbf{I}_0$. As a result, $\hat{I}_n = \cos \theta_n I_n = \mathcal{A}\hat{H}_r \cos \theta_n$.

REFERENCES

- [1] Z. Sun and I. F. Akyildiz, "Magnetic induction communications for wireless underground sensor networks," *IEEE Transactions on Antenna and Propagation*, vol. 58, no. 7, pp. 2426–2435, July 2010.
- [2] H. Guo, Z. Sun, and P. Wang, "Channel modeling of mi underwater communication using tri-directional coil antenna," in *IEEE Globecom 2015*, San Diego, USA, Dec 2015.
- [3] A. Karlsson, "Physical limitations of antennas in a lossy medium," *Antennas and Propagation, IEEE Transactions on*, vol. 52, no. 8, pp. 2027–2033, 2004.
- [4] H. Guo, Z. Sun, J. Sun, and N. M. Litchinitser, "M²i: Channel modeling for metamaterial-enhanced magnetic induction communications," *Antennas and Propagation, IEEE Transactions on*, vol. 63, no. 11, pp. 5072–5087, 2015.
- [5] J. B. Pendry, A. J. Holden, D. Robbins, and W. Stewart, "Magnetism from conductors and enhanced nonlinear phenomena," *Microwave Theory and Techniques, IEEE Transactions on*, vol. 47, no. 11, pp. 2075–2084, 1999.
- [6] C. Scarborough, Z. Jiang, D. Werner, C. Rivero-Baleine, and C. Drake, "Experimental demonstration of an isotropic metamaterial super lens with negative unity permeability at 8.5 mhz," *Applied Physics Letters*, vol. 101, no. 1, p. 014101, 2012.
- [7] R. W. Ziolkowski and A. D. Kipple, "Application of double negative materials to increase the power radiated by electrically small antennas," *IEEE Transactions on Antenna and Propagation*, vol. 51, no. 10, pp. 2626–2640, 2003.
- [8] A. Erentok and R. W. Ziolkowski, "Metamaterial-inspired efficient electrically small antennas," *Antennas and Propagation, IEEE Transactions on*, vol. 56, no. 3, pp. 691–707, 2008.
- [9] Y. Xie, J. Jiang, and S. He, "Proposal of cylindrical rolled-up metamaterial lenses for magnetic resonance imaging application and preliminary experimental demonstration," *Progress In Electromagnetics Research*, vol. 124, pp. 151–162, 2012.
- [10] W. Merrill, R. Diaz, M. Lore, M. Squires, and N. Alexopoulos, "Effective medium theories for artificial materials composed of multiple sizes of spherical inclusions in a host continuum," *IEEE Transactions on Antennas and Propagation*, vol. 47, no. 1, January 1999.
- [11] B. K. Horn, "Extended gaussian images," *Proceedings of the IEEE*, vol. 72, no. 12, pp. 1671–1686, 1984.
- [12] C. A. Balanis, *Antenna Theory*. John Wiley Publishing Company, 2005.
- [13] H. Guo and Z. Sun, "Channel and energy modeling for self-contained wireless sensor networks in oil reservoirs," *IEEE Transactions on Wireless Communications*, vol. 13, no. 4, pp. 2258–2269, April 2014.